Ab initio investigation of the affinity of novel bipyrazolate-based MOFs towards H2and CO2

CrystEngComm

PAPER

View Article Online
View Journal | View Issue

Cite this: *CrystEngComm*, 2015, **17**, 448

Ab initio investigation of the affinity of novel bipyrazolate-based MOFs towards H_2 and CO_2†

J. Baima,*[a] R. Macchieraldo,[a] C. Pettinari[b] and S. Casassa[a]

Received 29th September 2014,
Accepted 30th October 2014

DOI: 10.1039/c4ce01989j

www.rsc.org/crystengcomm

Two recently synthesized Zn and Cu tetramethyl-bipyrazole-based metal organic frameworks have been characterized and compared as regards their structural and electronic properties and their reactivity towards hydrogen and CO_2 molecules. *Ab initio* calculations have been performed on periodic models with the B3LYP hybrid and an empirical long-range dispersion correction. Interactions with the probe molecules in the two structures are almost iso-energetic and in all cases the physisorption becomes reversible as the temperature increases. Topological analysis of the electron density has been used to fully characterize the chemical bonding. On the basis of our study, it can be inferred that the experimentally observed larger adsorption capacity of the Cu framework is not ascribable to the strong interaction of the guest molecules with an exposed metal ion but to the higher number of adsorption sites and to the larger void volume.

1. Introduction

In the past decades, MOFs, a class of porous materials obtained by connecting metal ions (nodes) with organic molecules (linkers or spacers), have been intensively investigated because of the large number of potential technological applications,[1–9] descending directly from the possibility of modulating the macroscopic properties by varying the nature of the nodes and spacers. Among these properties, the most studied is indubitably the interaction with gas molecules for storage and separation applications. In particular, MOFs meeting the requirements for industrial hydrogen storage[10] or CO_2 capture and sequestration[11] could have a great impact on the energetic and environmental technologies in the near future.

Thousands of reports on novel MOFs have appeared over the past few years,[12] along with many in-depth investigations of their properties and functionality. Starting from the pioneering work on MOF-5,[13] the most well-known family of MOFs includes oxygen-donor ligands, mostly carboxylates, coupled to different metallic centers. Polyazolato-based ligands have been used as a means to build porous MOFs possessing a higher thermal and chemical stability than the carboxylato-based counterparts.[14–16]

A new family of bipyrazolate (BPZ)-based compounds, M(Me_4BPZ), M = Zn, Co, Cd, Cu, have been recently synthesized,[17] sharing the same ligand shown in Fig. 1. Their main features look very promising. TG analyses demonstrated that all of the four materials are thermally stable, decomposing in air above 600 K and preserving the thermal stability and framework topology throughout the consecutive heating–cooling series. Except for the Cd(II) derivative, they possess permanent porosity, with BET specific surface areas in the range of 83–396 $m^2\ g^{-1}$.

However, there is a large variability in the measured structural and adsorption properties within the group. In particular, Cu(Me_4BPZ) is not isoreticular with the other three, and this structural difference is associated with increased uptake of gas molecules and selectivity towards CO_2.[17] The increased CO_2 uptake could be attributed either to the larger void volume or to the presence of specific interactions with an open metal site in the latter framework. Cu ions are disposed in nodes of square shape, visible in Fig. 3, bonding with nitrogen atoms in a square planar coordination. A coordination vacancy is then accessible from the inside of the square. Open metal sites with coordination vacancies are considered highly desirable as they often play a key role in enhancing the adsorption of small molecules.[18–22] Nevertheless, it has already been demonstrated that the presence of exposed metals is not a guarantee of good adsorption

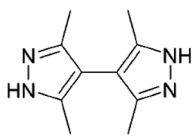

Fig. 1 3,3′,5,5′-Tetramethyl-4,4′-bipyrazole (Me_4BPZ in the following). Hydrogens are omitted.

[a] *Dipartimento Chimica IFM and Centre of Excellence NIS (Nanostructured Interfaces and Surfaces), Università degli Studi di Torino, via P. Giuria 5, I-10125 Torino, Italy*
[b] *School of Pharmacy, Università di Camerino, Italy. E-mail: jacopo.baima@unito.it*
† Electronic supplementary information (ESI) available. See DOI: 10.1039/c4ce01989j

capabilities, especially in azolate-based frameworks where the polarity of the ligand–metal bond is relatively low. Specifically, the capability to bond guest molecules can be signaled by a strong positive potential near the metal site.[23] Moreover, if the adsorption in Cu(Me$_4$BPZ) was driven by the under-coordinated metal ions, an even larger difference would be expected.[19,20]

More information about the chemical and physical reasons behind the difference between these two systems could prove important in directing the synthesis of new MOFs of this family towards better-performing compounds without sacrificing the thermal and chemical stability.

In this work, our aim is to compare the structural, electronic, and dielectric properties of two frameworks of the aforementioned group, namely, Zn(Me$_4$BPZ) and Cu(Me$_4$BPZ), by means of *ab initio* computational modeling and to investigate their affinity towards small gas molecules. The computational details are summarized in section II. Section III, Results, is subdivided into four parts; first, the periodic models of the two BPZ crystals will be described and their electronic features, dielectric properties and optical second harmonic generation will be presented. Then, the computed adsorption enthalpies of CO_2 and H_2 in both the structures will be discussed, and the bonding mechanism in different sites will be analyzed in detail. Finally, a topological analysis of the bonding framework, as proposed by Bader,[24] will be outlined, supporting the general results. Short conclusions and perspectives will be drawn in the last section.

2. Computational details

All of the calculations reported in the manuscript are performed with a developing version of the program Crystal for *ab initio* quantum chemistry of the solid state.[25,26] The hybrid DFT functional B3LYP[27,28] was adopted along with empirical corrections to include long-range dispersion effects, as proposed by Grimme[29] and modified for solid state systems.[30] All-electron basis sets, consisting of contracted Gaussian-type atomic orbital functions (AO), were used for all of the atoms. After a preliminary study to define the proper size for the basis set, metallic atoms were described by a modified TZVP basis set; for hydrogen, carbon, nitrogen, and oxygen, a Pople split valence 6-311G** basis set was used.

The condition for SCF convergence was set to 10^{-9} and 10^{-11} Hartree during geometry optimization and frequency calculation, respectively. The accuracy of the integral calculations was increased by setting the tolerances to 7 7 7 15 and 30. Reciprocal space is sampled regularly according to a sublattice with the shrinking factor set to 6, corresponding to 40 and 46 independent $\vec{k}$-points in the irreducible part of the first Brillouin zone in Zn(Me$_4$BPZ) and Cu(Me$_4$BPZ), respectively.

Full relaxation of the structures (both lattice parameters and atomic positions) was performed while keeping the symmetry of the system. Vibrational frequencies at the Γ point were calculated on the optimized geometry. Adsorption energies are corrected for the basis set superposition error[31] (BSSE) using the counterpoise method.[32] The electronic contributions to static polarizability and to first hyperpolarizability are evaluated through a Coupled Perturbed Kohn–Sham (CPKS) scheme.[33–36] The total static polarizability α_{ij} is the sum of the electronic and the vibrational contributions, so the dielectric tensor is:

$$\epsilon_{ij} = 1 + \frac{4\pi}{V}\left(\alpha_{ij}^{\mathrm{el}} + \alpha_{ij}^{\mathrm{vib}}\right) = 1 + \frac{4\pi}{V}\left(\alpha_{ij}^{\mathrm{el}} + \sum_{p}\frac{Z_{p,i}^{*}Z_{p,j}^{*}}{\nu_p^2}\right) \quad (1)$$

where ν_p is the vibrational frequency of mode p and $Z_{p,i}^{*}$ is the corresponding dynamic charge.

An updated version of the program TOPOND,[37,38] incorporated into the new version of the CRYSTAL code,[26] was employed to perform the charge density topological analysis, according to the Quantum Theory of Atoms In Molecules originally proposed for molecules by Bader[24] and subsequently extended to crystals (QTAIMAC).[39]

3. Results

3.1. Structures and spin states

Zn(Me$_4$BPZ) is isoreticular with the non-methylated counterpart and belongs to the tetragonal crystalline system with the space group $P\bar{4}2c$. The optimized structure is shown in Fig. 2. The metal ions are disposed in lines and are not sterically accessible. The optimized lattice parameters, listed in Table 1, are in agreement within 2% with the experimental data.

Cu(Me$_4$BPZ) has a much more complex structure due to the presence of a measure of conditioned disorder. The basic unit is organized around square-shaped Cu nodes connected

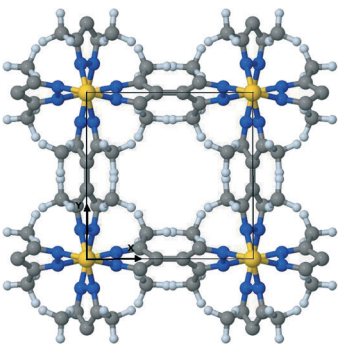

Fig. 2 Structure of Zn(Me$_4$BPZ). Zinc is represented in yellow, nitrogen in blue, carbon in grey and hydrogen in light grey.

Table 1 Structural data of the two BPZ frameworks. Experimental data are reported for the sake of comparison

		a/Å	c/Å	V/Å^3
Zn(Me$_4$BPZ)	Exp	8.8118	7.3668	572
	Opt	8.8027	7.2518	561
Cu(Me$_4$BPZ)	Exp	13.4612	13.4612	2439
	Opt	14.4926	11.6336	2444

by BPZ molecules. In ref. 17, two models are presented, one in which the Cu squares are parallel to each other and another with a 120° rotation between nearby squares, which avoid the superposition of methyl groups belonging to the same bipyrazole molecule. The correct disordered structure is similar to this one, but with no rigorous crystal periodicity in the 120° rotations. In both cases, however, the simulation indicates an additional tilting of the pyrazole rings in order to reduce the steric repulsion between methyl groups belonging to nearby molecules. This tilting also greatly reduces the steric repulsion associated with the first ordered model. For this reason, and because the neighborhood of the Cu squares is very similar between the two models, we have used the simpler structure in the following analysis, keeping in mind that the shape and size of the cages are influenced by the model and in both cases may differ from the real disordered system. The fact that the simulated cell volume (*Opt* row in Table 1) is in very good agreement with the one measured experimentally in the real sample suggests that this difference could be relatively small. The optimized structure is shown in Fig. 3.

The most stable spin configuration is anti-ferromagnetic, with an energy difference with respect to the ferromagnetic phase of 5.6 kJ mol^{-1} (twice the average thermal energy at room temperature).

3.2. Electronic and dielectric properties

The electronic density of states of $Zn(Me_4BPZ)$ and $Cu(Me_4BPZ)$ are shown in Fig. 4 and 5. Band structures are not shown, being flat and featureless. $Zn(Me_4BPZ)$ has a wide band gap of 5.44 eV, with both the highest occupied and the lowest unoccupied states belonging to C and N atoms in the pyrazole rings. $Cu(Me_4BPZ)$ has a lower gap of 2.32 eV due to the appearance of an unoccupied band localized mostly on the Cu atoms below the unoccupied states attributable to the pyrazole rings. These peculiarities can be appreciated by looking at the density of states projected on the AOs of the metals and nitrogen atoms of the empty structures, as described by the continuous black lines in Fig. 4 and 5, respectively.

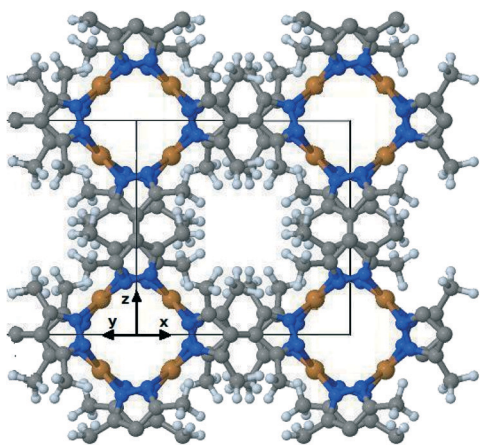

Fig. 3 Structure of $Cu(Me_4BPZ)$. Copper is represented in brown.

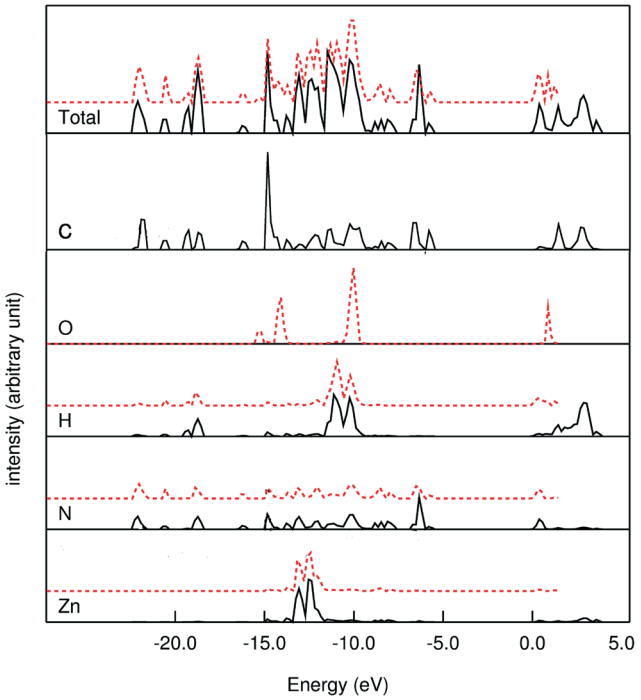

Fig. 4 Electronic density of states of the isolated (continuous black lines) and CO_2 interacting $Zn(Me_4BPZ)$ framework (dashed red lines). The projection on the nitrogen AOs, almost unaffected by the physisorption, demonstrates the band gap nature. Projections onto the AOs of the protons of the methyl groups and the oxygen involved in the formed hydrogen bonds are also reported in order to point out the subtle changes in the electron density.

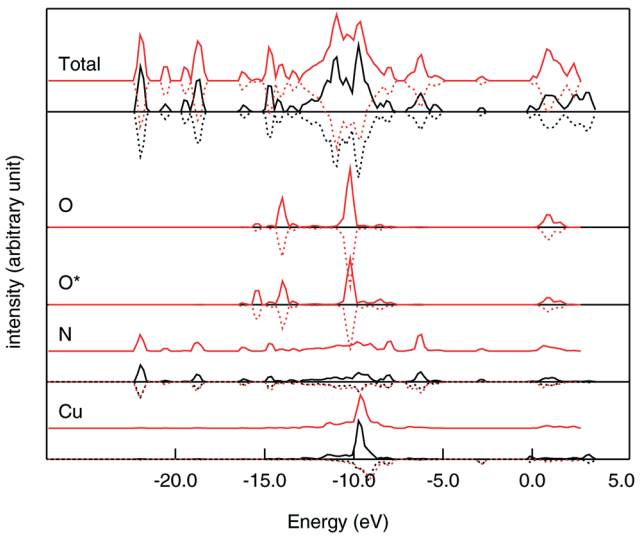

Fig. 5 Alpha (continuous lines) and beta (dashed lines) electronic density of states of the $Cu(Me_4BPZ)$ framework, both isolated (black lines) and interacting with CO_2 in the most favorable site (red lines). The oxygen marked with the asterisk is the one interacting with both the metal ions and the nitrogen atoms.

The dashed red lines snap the changes occurring as CO_2 uptake; in the Zn(Me$_4$BPZ) structure, a sensitive overlap between the AOs of both the molecular oxygens and the methyl protons is observed, as a result of an equal involvement of these two atoms in the hydrogen bond formation. Different features can be observed in Cu(Me$_4$BPZ), where only one of the molecular oxygen atoms interacts with the host lattice. In particular, the projections onto the AOs of the two oxygen atoms differ and the AOs of the interacting one present an overlap with the nitrogen and Cu electronic states in the upper valence band region.

Despite these differences, the dielectric constants of the two compounds, listed in Table 2, are similar, around the value of ε ~2.5. This is partly due to the larger void volume of Cu(Me$_4$BPZ) compensating for a larger polarizability. The value of ε is low enough for these systems to qualify as low dielectric constant materials,[40] but less so than other compounds of the same family.

MOFs are also widely recognized as having the potential to constitute a new generation of nonlinear optic materials.[9] Since both of the studied compounds lack an inversion center, it is interesting to extend the characterization to the second-order dielectric susceptibility $\chi^{(2)}$. The results are shown in Table 2: the values obtained for Zn(Me$_4$BPZ) are comparable with those of alpha-quartz, a traditional material for the study of second harmonic generation processes, but not high enough to be interesting in modern technological applications.

3.3. Adsorption

In the experimental investigation, a relevant difference was found between the affinity of the two systems for carbon dioxide. Since one of the main goals of MOF design is to obtain materials capable of selective adsorption of industrially and energetically relevant gases such as hydrogen and carbon dioxide, a correct interpretation of this difference can be extremely useful in designing new pyrazolate-based MOFs for storage applications. Fig. 7 shows that the open metal site present in the Cu(Me$_4$BPZ) crystal generates a sizable electrostatic potential despite the stability of the Cu–N bond. This can be interpreted as a further indication that the Cu ion is capable of anchoring guest molecules. On the other hand, Cu(Me$_4$BPZ) also has a larger number of adsorption sites for CO_2, as will be discussed in the following sections. An open metal site with polarizing power can be a favorable site for hydrogen adsorption, and thus despite the lack of experimental data in the case of H_2, both CO_2 and H_2 uptake have been explored.

In the following sections, adsorption enthalpies at T = 0 K and corresponding geometries are reported and discussed for each framework, while a more in-depth analysis of the nature of the bonding is left for section 3.4.

3.3.1. Zn(Me$_4$BPZ). In Zn(Me$_4$BPZ), the only sterically allowed adsorption site is inside the channels surrounded by methyl groups, so that there are no direct interactions with either the metal ions or the pyrazole rings. As could be expected from the flat electrostatic potential shown in Fig. 6, regardless of the initial position at the end of the optimization procedure, the probe molecules are situated in the middle of the channel, and it is possible to adsorb only one molecule per unit cell without significant repulsive intermolecular interactions. The guest molecule is surrounded by eight methyl groups, which screen the interaction with other parts of the framework.

In the case of H_2, the adsorption enthalpy, reported in Table 3, is quite low, as expected from the absence of specific adsorption sites or of a strong potential capable of polarizing the hydrogen molecule. In the case of CO_2, the enthalpy is relatively higher, and in fact not far from the values obtained for MOFs with much higher adsorption capacity.[21] This results from the collaborative binding with the methyl groups present within the interaction distance, as will be discussed in section 3.4. The inclusion of dispersion terms is crucial to stabilize the molecule physisorption; this is strong evidence of the quadrupolar nature of such an interaction between the guest molecules and the Zn(Me$_4$BPZ) cavity.

3.3.2. Cu(Me$_4$BPZ). There are two different kinds of adsorption sites in Cu(Me$_4$BPZ): (i) the electrostatically

Table 2 Band gap E_g, components of the static electronic and total polarizability tensors ε^e and ε^0, and second-order dielectric susceptibility $\chi^{(2)}$ for the two bipyrazolate MOFs studied. For both systems $\varepsilon^0_{yy} = \varepsilon^0_{xx}$, all other tensor components are zero or negligible

	Cu(Me$_4$BPZ)	Zn(Me$_4$BPZ)
E_g (eV)	2.32	5.44
ε^e_{xx}	2.75	2.36
ε^e_{zz}	2.49	2.51
ε^0_{xx}	3.07	2.82
ε^0_{zz}	3.21	2.12
$\chi^{(2)}_{xyz}$	0.07	−0.48

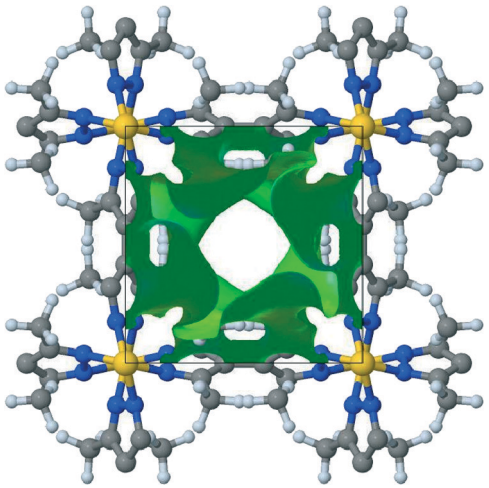

Fig. 6 Electrostatic potential of Zn(Me$_4$BPZ) projected on a charge density isosurface of 0.003 a.u. The color scale ranges from −0.073 (red) to 0.067 (blue) a.u.; the minimum and maximum values in this image are −0.019 and 0.026 respectively.

Table 3 Adsorption of CO_2 and H_2 in kJ mol^{-1}. ΔE is the electronic binding energy (at T = 0 K) corrected for BSSE. ΔH includes zero-point vibrational energy. ΔH_{B3lyp} does not include Grimme dispersion contributions

	Zn(Me$_4$BPZ)		Cu(Me$_4$BPZ)			
	CO_2	H_2	CO_2			H_2
			a	*b*	Channel	*a*
ΔE	−29.6	−8.8	−28.6	−25.6	−28.9	−5.9
ΔH (T = 0)	−22.1	−6.9	−23.4	−19.2	−21.5	−4.2
ΔH_{B3lyp} (T = 0)	17	2.6	34.0	23.2	14.2	3.8

charged area near the copper and nitrogen atoms and (ii) the apolar channels surrounded by methyl groups.

The apolar channels can accommodate up to two molecules per unit cell in equivalent positions, in a configuration similar to the Zn(Me$_4$BPZ) adsorption, where the surrounding methyl groups screen any interaction with other parts of the framework. As can be seen in Table 3, the adsorption energy is very similar to that of Zn(Me$_4$BPZ).

From the image of the electrostatic potential in Fig. 7, it is easily seen that it is possible for small molecules to access the zone of positive potential in the middle of the square formed by copper ions (the blue area in the bottom image) or the negative potential near the nitrogen atoms (red area). If the adsorbed molecules are closer to the nitrogen atoms, one molecule can be adsorbed on each side of the site with little expected lateral interaction. Five initial geometries have been tried in this area, namely, with the molecular axis pointing toward a Cu atom, toward the center of the Cu square, parallel to the diagonal and to the side of the Cu square, and close to the nitrogen atoms of the pyrazole rings. After geometry optimization, the non-binding and redundant configurations were discarded.

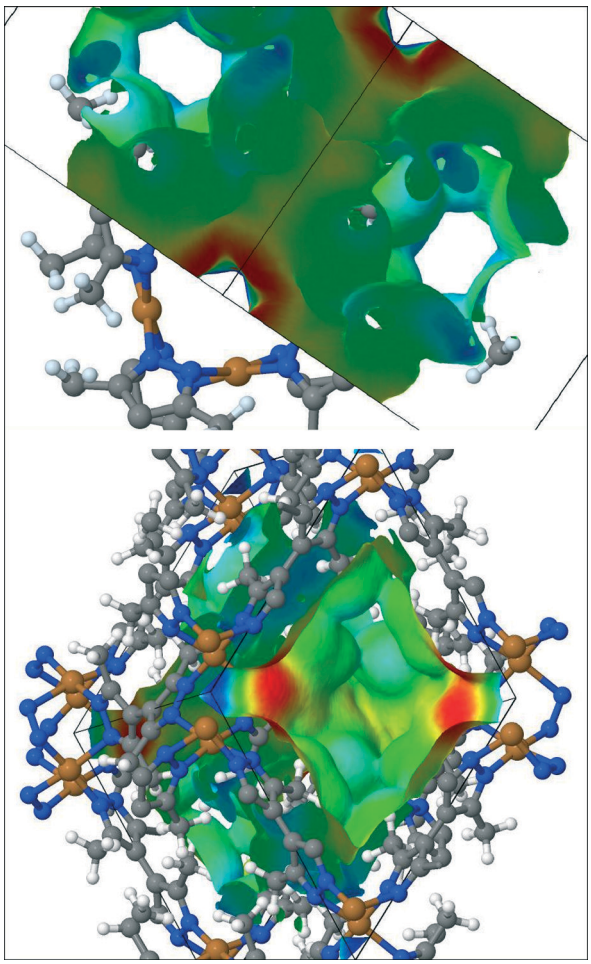

Fig. 7 Two views of the electrostatic potential of Cu(Me$_4$BPZ). The top figure shows the two different channels; in the bottom figure, the positive potential near the copper ions can be appreciated. Charge density value and color scheme for the potential are the same of Fig. 6.

For CO_2 adsorption, this left two inequivalent configurations; the images of the adsorption structures are provided in the ESI.† In the first one, labeled (a), the axis of the molecule is perpendicular to the Cu square shown in Fig. 3, with one oxygen close to the center of the square, at a distance of 2.57 Å from each Cu atom. In the second one, labeled (b), the axis of the molecule is parallel to the Cu square and the molecule is placed close to the pyrazole rings, so that the interaction between the molecular quadrupole and the nitrogen atoms, two at a distance of 3.3 Å from the carbon atom, appears important. Surprisingly, despite the stronger electrostatic potential in the region, the sites near the copper atoms have similar values of adsorption enthalpies to the apolar channels. In this case, however, the vibrational effects appear less relevant because of the less directional nature of the interaction.

The binding of H_2 is even weaker than in Zn(Me$_4$BPZ) and only occurs in a position similar to the (a) configuration of CO_2, but with the molecule placed directly in the middle of the copper atoms. The value of the adsorption energy suggests the complete absence of specific interactions.

3.4. Electron density topological analysis

From a preliminary observation of the electrostatic potential inside the cavities (see Fig. 6 and 7), it can be inferred that rather different interactions can take place between the hosted molecules and the surrounding crystalline framework. In fact, the cages look almost apolar for Zn(Me$_4$BPZ) and only one of the two Cu(Me$_4$BPZ) cavities presents zones of negative and positive potential in correspondence with nitrogen and copper atoms, respectively. The interaction energies are however quite similar. Then, in order to find out the force driving such physisorption processes, we have relied on the instruments provided by QTAIMAC analysis of the electron density, $\rho(\mathbf{r})$, as first proposed by Bader[24,41] and afterwards thoroughly improved by the contributions of many authors.[39,42,43] In particular, we aimed at: (i) investigating the formation of bonds between the host and the embodied molecules, (ii) sorting such interactions according to a chemistry classification and (iii) observing and reporting about any change in the crystalline and molecular bond topology as a consequence of physisorption.

Before discussing the results, we briefly recall the meaning of the main quantities used to analyze the atomic

interactions in QTAIMAC. The minima and maxima of $\rho(\mathbf{r})$, *i.e.* the points where its gradient vanishes, are defined as *critical points* (CP) and can be classified in terms of their rank r and signature s (the number of non-zero eigenvalues of the Hessian matrix in $\mathbf{r}_{CP}$ and the sum of their sign, respectively[24,37]). Of peculiar interest in the analysis of the bond nature are the *bond critical points* (B_{CP}), corresponding to (3, −1) in terms of the (r, s) notation, which represent a saddle in the electron density scalar field, with a local minimum along the atom–atom direction and two maxima in the directions perpendicular to it. In agreement with the most recent studies,[39] we will use the following topological indicators: the sign of the second derivative of the electron density (*i.e.* its Laplacian) $\nabla^2\rho(\mathbf{r})$, the adimensional $|V(\mathbf{r})|/G(\mathbf{r})$ ratio and the bond degree (BD) defined as $H(\mathbf{r})/\rho(\mathbf{r})$, as calculated using TOPOND[38] at each B_{CP} (here and in the following $\mathbf{r} \equiv \mathbf{r}_{B_{CP}}$, if not otherwise stated). $V(\mathbf{r})$ is the potential energy density, $G(\mathbf{r})$ is the positive definite kinetic energy and $H(\mathbf{r} = V(\mathbf{r}) + G(\mathbf{r}))$, the electron charge density, can be related to the Laplacian through the local expression of the virial theorem:

$$\frac{1}{4}\nabla^2\rho(\mathbf{r}) = V(\mathbf{r}) + 2G(\mathbf{r}) = H(\mathbf{r}) + G(\mathbf{r}) \quad (2)$$

Generally speaking, three classes of atomic interactions can be envisaged:[42] (i) a covalent bond (C) for which the sign of both the Laplacian and $H(\mathbf{r})$ is negative and due to a high concentration of density in the bond region ($V(\mathbf{r}) \gg G(\mathbf{r})$) the $|V(\mathbf{r})|/G(\mathbf{r})$ ratio is greater than 2; (ii) a transit bond (T) associated with a positive Laplacian, an almost zero value of BD and a value of $|V(\mathbf{r})|/G(\mathbf{r})$ between 1 and 2; and (iii) ionic, hydrogen bond and van der Waals interactions (I) for which both the Laplacian and $H(\mathbf{r})$ are positive and the electron kinetic energy at the B_{CP} is dominant with respect to $V(\mathbf{r})$, yielding a $|V(\mathbf{r})|/G(\mathbf{r})$ ratio less than unity.

The topological properties of the isolated systems, reported in Table 4, do not deserve any comments, the only concern being the interaction between the nitrogen atoms and the metal, classified as a transit bond. The bond framework of both the crystalline structures seems to be unaffected by the molecule uptake; the topology of the B_{CP}s between atoms close to the interacting region does not differ from the corresponding ones detailed in Table 4 and thus will not be reported. Even the *ring* structures, associated with (3, +1) CPs and indicating a region of charge depletion, are preserved when physisorption occurs.

However, some comments on the new bonding network are needed. The H_2 interaction in the Zn(Me_4BPZ) cage takes place through the formation of five weak hydrogen–hydrogen interactions with the protons of the neighboring methyl groups, three and two for each atom. The adsorption completely preserves the molecular nature and the covalency of the bond, as can be inferred by comparing the values of the topological descriptors for the isolated and interacting molecule reported in Tables 4 and 5, respectively (refer to the H–H bond). Topological analysis confirms the van der Waals nature of the adsorption. Also, in the case of CO_2, the molecule interacts with the hydrogens of the closest methyl groups, giving rise to a total of eight weak hydrogen bonds, four per oxygen. Despite the weakness of these bonds, the number of interactions is enough to generate a noticeable adsorption energy.

In Cu(Me_4BPZ), where the metal sites are more exposed, a more directional interaction takes place between one of the H_2 protons and the metal ion, yielding a sensitive asymmetry in the homonuclear molecular bond, as can be seen by looking at the net atomic charges on H_2 collected in Table 6. Nevertheless, in agreement with the value of the BD involving the hydrogen, (H/ρ being 0.2 and 0.03, respectively) the strength of the interaction is less pronounced than in the Zn(Me_4BPZ) MOF.

Table 4 Bond critical points (B_{CP}) of the electron density for the isolated systems. All the data, but the dimensionless $|V|/G$ ratio, are expressed in a.u. *C*, *T* and *I* stand for covalent, transit and ionic interactions, respectively. Q^* is the atomic net charge as evaluated by the integration of the electron density over the atomic basins and refers to the atom labeled with the asterisk[24]

System	Bond	ρ	$\nabla^2\rho$	H/ρ	$\lvert V\rvert/G$	Q^*	Type
H_2	H^*–H^*	0.261	−1.055	−1.011	≫2	≈0.0	*C*
CO_2	C–O^*	0.457	−0.022	−1.769	2.0	−1.067	*C*
Zn(Me_4BPZ)	Zn–N	0.084	0.370	−0.220	1.2		*T*
	N–N	0.356	−0.639	−0.952	2.9		*C*
	C–H	0.278	−0.931	−0.998	7.2		*C*
Cu(Me_4BPZ)	Cu^*–N	0.100	0.383	−0.341	1.3	1.058	*T*
	N–N^*	0.361	−0.656	−0.964	2.9	−0.719	*C*
	C–H	0.278	−0.935	−0.989	7.6		*C*

Table 5 B_{CP} for Zn(Me_4BPZ) interacting with molecules. Symbols and units as in Table 4. The values of the C–O B_{CP} refer to the oxygen involved in the hydrogen bond with the lattice protons. Q values for the molecular atoms are reported. In the case of H_2, a feeble charge flow from one proton to the other is observed, as indicated by the different sign of the net charge and their absolute value being very close to zero. Oxygens show an equal increase of 2% in their net charge correlated with a corresponding gain of 3% in their atomic volume

Zn	Bond	ρ	$\nabla^2\rho$	H/ρ	$\lvert V\rvert/G$	Q^*
+H_2	H^*–H^*	0.263	−1.064	−1.014	≫2	−0.013/0.015
	H⋯H	0.003	0.012	0.202	0.7	
+CO_2	C–O^*	0.459	−0.007	−1.625–1.773	2.0	−1.083/−1.087
	H⋯O	0.005	0.019	0.219	0.7	

Table 6 B_{CP} for Cu(Me_4BPZ) interacting with H_2 and CO_2 in the most favorable site. Symbols and units as in Table 4. Q values are reported for the molecular hydrogens and for all the interacting atoms in the case of the CO_2 uptake

Cu	Bond	ρ	$\nabla^2\rho$	H/ρ	$\lvert V\rvert/G$	Q^*
+H_2	H–H	0.293	−1.329	−1.143	≫2	−0.080/0.099
	Cu⋯H	0.017	0.053	0.030	0.9	
+CO_2	C–O^*	0.443	−0.183	−1.745	2.1	−0.410/−0.174
	Cu^*⋯O	0.020	0.084	0.065	0.9	1.080
	N^*⋯O	0.016	0.063	0.139	0.8	−0.773

As regards the CO_2 adsorption in its most favorable site, two kinds of bonds, both classifiable as belonging to the transit region and involving the same molecular oxygen, take place: with the four copper atoms and the four nitrogen atoms, respectively. A detectable degree of charge transfer can be observed from the metals through the CO_2 oxygen and back to the lattice nitrogen atoms, indicating a redistribution of the charge on the whole molecule and a sensitive change in the framework charge.

4. Conclusions

In this work, we have analyzed by *ab initio* simulations the structural, dielectric and adsorption properties of two recently synthesized metal organic frameworks with tetramethylbipyrazolate linkers connecting the copper and zinc ions.[17] Heats of physisorption of CO_2 and H_2 inside the micropores are reported as calculated with a hybrid DFT functional augmented with an empirical dispersion correction. Dispersive contributions are shown to be of fundamental importance in predicting the correct geometries and energies. Topological analysis of the electron density has been used to understand the nature of the interactions between the host lattice and the molecules.

The connection between the differences in the structure and adsorption capabilities of the materials has been discussed. Despite the presence of an open metal site, the interactions of the Cu-based framework with both the probe molecules are not qualitatively stronger with respect to the Zn-based structure. For H_2, the interactions with both frameworks are rather unspecific and weak. For CO_2, in both structures a weak interaction with the protons of the methyl groups is present. The interaction with the open Cu site is only marginally stronger, despite the presence of a region of positive electrostatic potential near the metal ions that could suggest the capability to bond guest molecules. From the presence of open metal sites, however, results the higher number of adsorption sites available, which explains the increased selectivity towards CO_2 of Cu(Me_4BPZ). This result is a confirmation that, as was already found in the past with different metals,[23] open metal sites showing strong bonds with the ligands such as metal–azolate bonds are likely to display significantly weaker interactions with adsorbed molecules with respect to those found in carboxylate frameworks, possibly comparable to unspecific and dispersive interactions.

Acknowledgements

The authors would like to thank Prof. Simona Galli for providing the structural data of the Cu(Me_4BPZ) crystalline structure. The present work has received financial support in the framework of the PRIN2010 project DESCARTES. Computer facilities from the PRACE project on SuperMUC are gratefully acknowledged.

References

1 M. S. Silverstein, N. R. Cameron and M. A. Hillmyer, *Porous polymers*, Wiley, 2011.
2 H. Li, M. Eddaoudi, M. O'Keeffe and O. M. Yaghi, *Nature*, 1999, **402**, 276.
3 M. P. Suh, H. J. Park, T. K. Prasad and D. Lim, *Chem. Rev.*, 2012, **112**, 782.
4 M. Yoon, R. Srirambalaji and K. Kim, *Chem. Rev.*, 2012, **112**, 1196.
5 Y. Cui, Y. Yue, G. Qian and B. Chen, *Chem. Rev.*, 2012, **112**, 1126.
6 M. Kurmoo, *Chem. Soc. Rev.*, 2008, **38**, 1353.
7 W. Zhang and R. Xiong, *Chem. Rev.*, 2012, **112**, 1163.
8 P. Horcajada, R. Gref, T. Baati, P. K. Allan, G. Maurin, P. Couvreur, G. Férey, R. E. Morris and C. Serre, *Chem. Rev.*, 2012, **112**, 1232.
9 C. Wang, T. Zhang and W. Lin, *Chem. Rev.*, 2011, **112**, 1084.
10 S. Satyapal, J. Petrovic, C. Read, G. Thomas and G. Ordaz, *Catal. Today*, 2007, **120**, 246.
11 K. Sumida, D. L. Rogow, J. A. Mason, T. M. McDonald, E. D. Bloch, Z. R. Herm, T.-H. Bae and J. R. Long, *Chem. Rev.*, 2011, **112**, 724.
12 N. W. Ockwig, O. Delgado-Friedrichs, M. O'Keeffe and O. M. Yaghi, *Acc. Chem. Res.*, 2005, **38**, 176.
13 H. Li, M. Eddaoudi, M. O'Keeffe and O. M. Yaghi, *Nature*, 1999, **402**, 276.
14 J. P. Zhang, Y. B. Zhang, J. B. Lin and X. M. Chen, *Chem. Rev.*, 2012, **112**, 1001.
15 J. H. Cavka, S. Jakobsen, U. Olsbye, N. Guillou, C. Lamberti, S. Bordiga and K. P. Lillerud, *J. Am. Chem. Soc.*, 2008, **130**, 13850.
16 V. Colombo, S. Galli, H. J. Choi, G. D. Han, A. Maspero, G. Palmisano, N. Masciocchi and J. R. Long, *Chem. Sci.*, 2011, **2**, 1311.
17 A. Tabacaru, C. Pettinari, I. Timokhin, F. Marchetti, F. Carrasco-Marín, F. J. Maldonado-Hodar, S. Galli and N. Masciocchi, *Cryst. Growth Des.*, 2013, **13**, 3087.
18 M. Eddaoudi, D. B. Moler, H. Li, B. Chen, T. M. Reineke, M. O'Keeffe and O. M. Yaghi, *Acc. Chem. Res.*, 2001, **34**, 319.
19 D. M. D'Alessandro, B. Smit and J. R. Long, *Angew. Chem., Int. Ed.*, 2010, **49**, 6058.
20 S. Bordiga, L. Regli, F. Bonino, E. Groppo, C. Lamberti, B. Xiao, P. S. Wheatley, R. E. Morris and A. Zecchina, *Phys. Chem. Chem. Phys.*, 2007, **9**, 2676.
21 L. Grajciar, A. D. Wiersum, P. L. Llewellyn, J.-S. Chang and P. Nachtigall, *J. Phys. Chem. C*, 2011, **115**, 17925.
22 Q. Yang and C. Zhong, *J. Phys. Chem. B*, 2006, **110**, 655.
23 E. Albanese, B. Civalleri, M. Ferrabone, F. Bonino, S. Galli, A. Maspero and C. Pettinari, *J. Mater. Chem.*, 2012, **22**, 22592.
24 R. F. W. Bader, Atoms in Molecules - A Quantum Theory, *International Series of Monographs in Chemistry*, Oxford University Press, Oxford, UK, 1990, vol. 22.
25 R. Dovesi, V. R. Saunders, C. Roetti, R. Orlando, C. M. Zicovich-Wilson, F. Pascale, B. Civalleri, K. Doll, N. M. Harrison, I. J. Bush, P. D'Arco, M. Llunell, M. Causà and Y. Noel, *CRYSTAL 2014 User's Manual*, 2014.

26 R. Dovesi, R. Orlando, A. Erba, C. M. Zicovich-Wilson, B. Civalleri, S. Casassa, L. Maschio, M. Ferrabone, M. D. laPierre, P. D. Arco, Y. Noël, M. Causà, M. Rerat and B. Kirtman, *Int. J. Quantum Chem.*, 2014, **114**, 1287.
27 A. D. Becke, *J. Chem. Phys.*, 1993, **98**, 5648.
28 C. Lee, W. Yang and R. G. Parr, *Phys. Rev. B: Condens. Matter Mater. Phys.*, 1988, **37**, 785.
29 S. Grimme, *J. Comput. Chem.*, 2006, **27**, 1787.
30 B. Civalleri, C. M. Zicovich-Wilson, L. Valenzano and P. Ugliengo, *CrystEngComm*, 2008, **10**, 405.
31 S. F. Boys and F. Bernardi, *Mol. Phys.*, 1970, **19**, 553.
32 E. R. Davidson and D. Feller, *Chem. Rev.*, 1986, **86**, 681.
33 G. J. B. Hurst, M. Dupuis and E. Clementi, *J. Chem. Phys.*, 1988, **89**, 385.
34 B. Kirtman, F. L. Gu and D. M. Bishop, *J. Chem. Phys.*, 2000, **113**, 1294.
35 M. Ferrero, M. Rérat, R. Orlando and R. Dovesi, *J. Chem. Phys.*, 2008, **128**, 014110.
36 M. Ferrero, M. Rérat, B. Kirtman and R. Dovesi, *J. Chem. Phys.*, 2008, **129**, 244110.
37 C. Gatti, V. R. Saunders and C. Roetti, *J. Chem. Phys.*, 1994, **101**, 10686.
38 C. Gatti and S. Casassa, *TOPOND-2013: an electron density topological program for systems periodic in N (N = 0–3) dimensions, User's manual*, CNR-CSRSRC, Milano, 2013.
39 C. Gatti, *Z. Kristallogr.*, 2005, **220**, 399.
40 W. Volksen, R. D. Miller and G. Dubois, *Chem. Rev.*, 2009, **110**, 56.
41 R. F. W. Bader and H. Essen, *J. Chem. Phys.*, 1984, **80**, 1943.
42 E. Espinosa, I. Alkorta, J. Elguero and E. Molins, *J. Chem. Phys.*, 2002, **117**, 5529.
43 P. Macchi and A. Sironi, *Coord. Chem. Rev.*, 2003, **238–239**, 383.